Dopazo C, Cifuentes L, Alwazzan D, Chakraborty N.

Influence of the Lewis number on effective strain rates in weakly turbulent premixed combustion.

***Combustion Science and Technology* (2017)**

DOI: https://doi.org/10.1080/00102202.2017.1398744

Influence of the Lewis number on effective strain rates in weakly turbulent premixed combustion

Cesar Dopazo[1], Luis Cifuentes[2], Dana Alwazzan[3], Nilanjan Chakraborty[3]

[1] School of Engineering and Architecture - Fluid Mechanics Area, University of Zaragoza, C/Maria de Luna 3 Zaragoza, Spain

[2]Institute for Combustion and Gasdynamics (IVG), University of Duisburg-Essen, Duisburg 47048, Germany

[3] School of Mechanical and Systems Engineering, Newcastle University, Newcastle-Upon-Tyne, NE1 7RU, UK

ABSTRACT

The influence of the global Lewis number, *Le*, on the statistical behaviour of the 'effective' normal and tangential strain rates have been analysed based on three-dimensional DNS data of freely propagating statistically planar turbulent premixed flames with *Le* = 0.34, 0.60, 0.80, 1.00 and 1.20. The volumetric dilatation rate is found to be mostly positive and its magnitude increases with decreasing *Le*. The flow normal strain rate predominantly assumes positive values and thus tends to pull adjacent iso-scalar surfaces apart, which reduces scalar gradients. By contrast, the "added" normal strain rate due to derivatives of the displacement speed normal to iso-surfaces has the propensity to push them closer together, and therefore increase the magnitude of scalar gradients. The balance between flow and added normal strain rates along with the advective transport determines whether scalar gradients are enhanced or destroyed. Iso-surface elementary area stretching by the fluid flow increases with decreasing Lewis number, and the added tangential strain rate exhibits predominantly negative values and is determined by the correlation between displacement speed components and flame curvature. It has been found that turbulent flames with small values of Lewis number exhibit flame thinning and high values of the flame surface area and these tendency strengthens with decreasing Lewis number. This behaviour has been explained in detail in terms of the statistical behaviours of effective normal and tangential strain rates.

Keywords: Iso-scalar non-material surfaces, flow, "added" and "effective" normal and tangential strain rate, volumetric dilation rate, Direct Numerical Simulation, premixed flames

1. INTRODUCTION

Direct Numerical Simulation (DNS) of turbulent premixed flames is a powerful tool to understand complex interactions of a flame with the small-scale geometry of the scalar field and the fine flow structures. Recent DNS dataset examinations (Cifuentes *et al*., 2014; Cifuentes *et al*., 2015; Dopazo *et al*., 2015a; Dopazo and Cifuentes, 2016 and references therein) have analysed the mechanisms, which affect the evolution of the normal distance separating two adjacent iso-scalar surfaces in turbulent premixed combustion. The reaction progress variable c could be used to identify iso-surfaces in turbulent premixed flames. Turbulence-scalar interactions can be characterised by the flow normal, a_N , and tangential, a_T , strain rates, which add up to the volumetric dilatation rate, and by the "added" tangential, $2S_d k_m$, and normal, $\partial S_d/\partial x_N$, strain rates, arising due to the non-material nature of c −iso-surfaces (i.e., flame propagation), where S_d is the local displacement speed on an iso-surface relative to the fluid velocity. The quantity $2S_d k_m$ is a curvature-induced tangential strain rate, where k_m is the mean of principal curvatures of the c −iso-surface, $\partial S_d/\partial x_N$ accounts for variations in propagation velocities of different iso-scalar surfaces in their normal direction with the local flame normal coordinate x_N being positive towards the fresh reactants. The quantities S_d and $\partial S_d/\partial x_N$ arise due to the combined action of molecular diffusion and chemical conversion. Summation of flow and added strain rates gives rise to the "effective" tangential, $a_T^{eff} = a_T + 2\,k_m S_d$, (usually, termed flame stretch factor), and normal, $a_N^{eff} = a_N + \partial S_d/\partial x_N$, strain rates. The effective strain rates, a_T^{eff} and a_N^{eff} , determine the unitary time rate of change of the infinitesimal surface area on $c(\mathbf{x}, t) = const$ and of the distance between two adjacent iso-scalar surfaces. Pope (1988) investigated the evolution of non-material iso-surfaces using parametric coordinates and derived, among other things, an expression for the surface stretch factor; the latter is commonplace in turbulent combustion studies (Chung and Law, 1984; Candel and Poinsot, 1990; Veynante and Vervisch, 2002). A

number of publications (Vervisch *et al*., 1995; Kollmann and Chen, 1998; Chakraborty and Cant, 2005a; Sankaran *et al*., 2007; Kim and Pitsch, 2007; Chakraborty and Swaminathan, 2007; Chakraborty and Klein, 2008; Chakraborty *et al*., 2008; Chakraborty *et al*., 2009) analysed an evolution equation for the modulus of the reaction progress variable gradient to determine the gradient growth or reduction; furthermore, some authors obtained different contributions of $\partial S_d/\partial x_N$ to the gradient budget conditional on the mean curvature.

Chakraborty and co-workers (Chakraborty and Swaminathan, 2007; Chakraborty and Klein, 2008; Chakraborty *et al*., 2009) obtained, via DNS of turbulent premixed flames, positive values of a_N in the "corrugated flamelets" regime and negative ones in the "thin reaction zone regime". They analysed the Lewis number effects on the scalar gradient alignment and found, that mainly for positive values of a_N, "the most extensive principal strain rate" is preferentially perpendicular to iso-scalar surfaces and "destroys the scalar gradient". Dopazo et *al.* (2015a,b) identified the effective normal strain rate as responsible for different scalar gradient evolutions; they showed, via examination of existing DNS datasets for low Karlovitz number and *Le* =1.0, that a_N is consistently positive (reducing scalar gradients), whereas the added normal strain rate is negative (i.e., iso-scalar surfaces increase their propagation speed relative to the fluid towards the hot products, causing two of them to approach each other) and, therefore, tend to enhance scalar gradients. The flame propagation contribution is apparently the dominant one. Kim and Pitsch (2007) and Chakraborty and Klein (2008) recast the normal strain rate contribution of the scalar gradient transport equation in terms of volumetric dilatation and tangential strain rates; they have examined DNS data to analyse the statistics of the reaction progress variable gradient transport, and the joint PDFs of either flow dilatation or tangential strain rate and mean curvature have been discussed.

To the best of our knowledge, a detailed analysis of the effects of Lewis number on the effective tangential and normal strain rates has never been reported. This work aims at exploring the importance of the effective tangential and normal strain rates in mixing in turbulent premixed flames. Section 2 introduces the mathematical description of the turbulent mixing problem and summarizes the kinematics of non-material iso-scalar surfaces. A brief description of the numerical implementation, pertaining to the DNS database considered here, is presented in Section 3. Section 4 analyzes the results and discusses their physical significances and implications. Some concluding remarks and suggestions for future work are finally presented in Section 5.

2. MATHEMATICAL CONCEPTS

The reaction progress variable, $c(\mathbf{x}, t)$ increases monotonically from 0 in the unburned gas to 1 in fully burned products, and it is governed by the convection-diffusion-reaction conservation equation,

$$\frac{\partial c}{\partial t} + u_j \frac{\partial c}{\partial x_j} = \frac{1}{\rho}\frac{\partial}{\partial x_j}\left(\rho D \frac{\partial c}{\partial x_j}\right) + \dot{\omega}_c, \tag{1}$$

where u_j is the j^{th} component of the flow velocity vector, ρ is the fluid density, D is the Fickian molecular diffusivity coefficient for c and $\dot{\omega}_c$ stands for its net production rate by chemical reaction. The molecular diffusion term can be expanded into its normal and tangential components (Peters *et al*., 1998; Echekki and Chen, 1999; Chakraborty and Cant, 2005a,b; Chakraborty and Swaminathan, 2007; Chakraborty *et al*., 2008):

$$\frac{1}{\rho}\frac{\partial}{\partial x_j}\left(\rho D \frac{\partial c}{\partial x_j}\right) = \frac{1}{\rho}\frac{\partial}{\partial x_N}\left(\rho D \frac{\partial c}{\partial x_N}\right) + 2k_m D \frac{\partial c}{\partial x_N}, \tag{2}$$

The local unit vector, $\boldsymbol{N}$, normal to the iso-scalar surface $c(\mathbf{x}, t) = const$, pointing toward the fresh reactants, is given by,

$$N_i = -\frac{1}{|\nabla c|}\frac{\partial c}{\partial x_i}. \tag{3}$$

The magnitude of the gradient of c is $|\nabla c| = -\partial c/\partial x_N$, and the mean of the principal curvatures of the iso-surface is $k_m = 0.5(\partial N_j/\partial x_j)$. According to the convention followed here, the flame elements which are convex (concave) towards the reactants have positive (negative) curvature values.

If the propagation velocity, $\boldsymbol{v^c}(\boldsymbol{x}, t)$, of a point **x** of the iso-surface at time t is expressed as $\boldsymbol{v^c}(\boldsymbol{x}, t) = \boldsymbol{u}(\boldsymbol{x}, t) + S_d(x, t)\boldsymbol{N}(\boldsymbol{x}, t)$, Eq. (1) can alternatively be written as:

$$\frac{\partial c}{\partial t} + u_j \frac{\partial c}{\partial x_j} = -S_d \frac{\partial c}{\partial x_N}\,. \tag{4}$$

Here, S_d is the local displacement speed of the iso-surface relative to the flow velocity. Equating the right sides of Eqs. (1) and (4), an expression for the displacement speed is obtained, namely,

$$S_d = \underbrace{-\frac{1}{(\partial c/\partial x_N)}\left[\frac{1}{\rho}\frac{\partial}{\partial x_N}\left(\rho D \frac{\partial c}{\partial x_N}\right)\right]}_{S_n} \underbrace{-2Dk_m}_{S_t} \underbrace{-\frac{\dot{\omega}_c}{(\partial c/\partial x_N)}}_{S_r}\,. \tag{5}$$

The derivative $\partial S_d/\partial x_N$ can obtained as:

$$\frac{\partial S_d}{\partial x_N} = \underbrace{\frac{\partial}{\partial x_N}\left\{-\frac{1}{(\partial c/\partial x_N)}\left[\frac{1}{\rho}\frac{\partial}{\partial x_N}\left(\rho D \frac{\partial c}{\partial x_N}\right)\right]\right\}}_{(\partial S_n/\partial x_N)} \underbrace{+\frac{\partial(-2Dk_m)}{\partial x_N}}_{(\partial S_t/\partial x_N)} \underbrace{+\frac{\partial}{\partial x_N}\left[\frac{-\dot{\omega}_c}{(\partial c/\partial x_N)}\right]}_{(\partial S_r/\partial x_N)}\,. \tag{6}$$

The three terms on the right sides of Eqs. (5) and (6) quantify the contributions of normal and tangential (due to curvature) molecular diffusions and chemistry, respectively.

Time rates of change of a non-material infinitesimal vector magnitude, $\boldsymbol{r} = (\Delta x_N)\boldsymbol{N}$ (joining two points on adjacent iso-surfaces, $c(\boldsymbol{x}, \mathrm{t}) = \Gamma$ and $c(\boldsymbol{x}, \mathrm{t}) = \Gamma + \Delta\Gamma$), a surface area element, A (on the iso-surface $c(\boldsymbol{x}, \mathrm{t}) = \Gamma$), and an infinitesimal volume, V = A(Δx_N), have been previously obtained (Dopazo *et al*., 2015a,b; Dopazo and Cifuentes, 2016):

$$\frac{1}{\Delta x_N}\frac{d\Delta x_N}{dt} = a_N + \frac{\partial S_d}{\partial x_N}\,, \tag{7}$$

$$\frac{1}{A}\frac{dA}{dt} = a_T + 2k_m S_d, \tag{8}$$

$$\frac{1}{V}\frac{dV}{dt} = a_N + \frac{\partial S_d}{\partial x_N} + a_T + 2k_m S_d \ . \tag{9}$$

$a_N = N_i S_{ij} N_j$ and $a_T = \left(\delta_{ij} - N_i N_j\right) S_{ij}$ are the flow strain rates normal and tangential, respectively, to the iso-surface, $S_{ij} = 0.5(\partial u_i/\partial x_j + \partial u_j/\partial x_i)$ is the flow strain rate tensor. The effective normal and tangential strain rates are:

$$a_N^{eff} = a_N + \frac{\partial S_d}{\partial x_N} \ , \tag{10}$$

and

$$a_T^{eff} = a_T + 2k_m S_d \ . \tag{11}$$

The flow volumetric dilatation rate is $\nabla \cdot \boldsymbol{u} = a_N + a_T$. The added normal, $\partial S_d/\partial x_N$, and tangential, $2k_m S_d$, strain rates, respectively, are caused by the nonmaterial nature of curved iso-surfaces, which propagate with a speed relative to the fluid, S_d, varying with x_N. Whereas, Eq. (8) has been derived by several investigators (Chung and Law, 1984; Pope, 1988; Candel and Poinsot, 1990; Veynante and Verviscvh, 2002), Eqs. (7) and (9) have not been used in the literature. All terms in Eq. (7) have dimensions of an inverse of time. In principle, $(1/\Delta x_N)(\, dx_N/dt)$ can be considered inversely proportional to the characteristic mixing time, mainly depending on the value of the Karlovitz number. Eq. (7) dictates how scalar gradient and dissipation rate evolve, and also governs the characteristic mixing times associated with molecular diffusion rates and chemical conversion rates. Depending on the Karlovitz number the characteristic mixing time will be determined either by the Kolmogorov time micro-scale or by the thermochemical times. The implementation in the molecular mixing models of the dimensional or dimensionless equations for the time rate of change of the infinitesimal distance between two adjacent iso-surfaces is one of the main modelling challenges in the analysis of turbulent premixed combustion. The potential of that equation is yet to be exploited. Eq. (9) is related to the flow volumetric dilatation rate of non-material volume elements of flames and to

the mass entrainment rate per unit mass into those volumes. Once again, the potential of Eq. (9) is yet to be explored and exploited. The present analysis cocentrates on the influences of global Lewis number on the statistical behaviours of the effective strain rates a_N^{eff} and a_T^{eff} and their various components along with their implications on the evolution of $|\nabla c|$. These statistics play pivotal roles in the development of high-fidelity closures of generalised Flame Surface Density (FSD=$\Sigma_{gen} = \overline{|\nabla c|}$) and Scalar Dissipation Rate (SDR=$N_c = D|\nabla c|^2$) (Boger *et al*., 1998; Vervisch and Veynante, 2002).

While a_T^{eff} determines the effective flame or area stretch factor, a_N^{eff} controls the enhancement or destruction of scalar-gradients. Derivation of Eq. (4) with respect to x_i yields

$$\frac{\partial c_{,i}}{\partial t} + u_j \frac{\partial c_{,i}}{\partial x_j} = -u_{j,i} c_{,j} - \frac{\partial S_d}{\partial x_i}\frac{\partial c}{\partial x_N} - S_d \frac{\partial c_{,i}}{\partial x_N} \tag{12}$$

where $c_{,i}$ stands for $c_{,i} = \partial c/\partial x_i$. Multiplication by $c_{,i}$ leads, after simple algebra, to

$$\frac{1}{|\nabla c|}\left(\frac{\partial |\nabla c|}{\partial t} + v_j^c \frac{\partial |\nabla c|}{\partial x_j}\right) = -a_N^{eff} \tag{13}$$

Eq. (13) is the time rate of change of $|\nabla c|$ per unit of $|\nabla c|$ following the nonmaterial iso-surface. If $a_N^{eff} < 0$ ($a_N^{eff} > 0$) the first term of the right side of Eq. (13) enhances (destroys) scalar-gradients.

Replacing v_j^c in Eq. (13) by $u_j(\boldsymbol{x}, t) + S_d(x, t)N_j(\boldsymbol{x}, t)$ yields the form in terms of the material derivative, namely,

$$\frac{1}{|\nabla c|}\left(\frac{\partial |\nabla c|}{\partial t} + u_j \frac{\partial |\nabla c|}{\partial x_j}\right) = -a_N^{eff} - S_d \frac{1}{|\nabla c|}\frac{\partial^2 c}{\partial x_N^2} \tag{14}$$

A steady planar laminar premixed flame is the simplest illustration of the a_N^{eff} concept. The flow velocity of two adjacent iso-c planes, $c(x,t) = \Gamma$ and $c(x,t) = \Gamma + \Delta\Gamma$, separated by a distance Δx_N, within the flame structure, are $u(x)$ and $u(x) + [du(x)/dx]\Delta x_N$, where x is the

coordinate pointing toward the combustion products (opposite sense of x_N). Since the two iso-surfaces do not move $u(x) = S_d(x)$ and $du(x)/dx = dS_d(x)/dx$. Therefore, to have a steady flame the displacement speed relative to the fluid, $S_d(x)$, must vary with x. In this example $du(x)/dx$ is the flow normal strain rate, whereas $-dS_d(x)/dx = dS_d(x)/dx_N$ is the "added" normal strain rate. For this steady flame $a_N^{eff} = 0$, and Eq. (13) is identically satisfied.

3. DESCRIPTION OF DNS DATA

A widely used DNS database (Chakraborty and Klein, 2008; Chakraborty *et al*., 2009; Chakraborty and Cant, 2009,2011; Chakraborty and Swaminathan, 2010; Chakraborty *et al*., 2011; Katragadda and Chakraborty, 2012; Katragadda *et al*., 2012; Chakraborty and Lipatnikov, 2013; Chakraborty *et al*., 2014; Gao *et al*., 2014; Gao *et al*., 2015; Klein *et al*., 2016; Chakraborty *et al*., 2016) of freely propagating statistically planar flames with global Lewis number $Le = 0.34$, 0.6, 0.8, 1.0 and 1.2 has been considered for this analysis so that the effects of global Lewis number on the statistical behaviours of the effective strain rates can be analysed in isolation. Several previous theoretical (Sivashinsky, 1977; Clavin and Williams, 1982) and numerical (Ashurst *et al*., 1988; Haworth and Poinsot, 1992; Rutland and Trouvé, 1993; Trouvé and Poinsot, 1994; Han and Huh, 2008) analyses used simple chemistry and modified Lewis number independently of other parameters in order to analyse the effects of differential diffusion arising from non-unity Lewis number in isolation; the same approach has been adopted in this analysis. Moreover, the models proposed based on *a priori* DNS analyses using this database (Katragadda *et al*., 2012; Gao *et al*., 2014; Gao *et al*., 2015; Klein *et al*., 2016) have been found to be in good agreement with *a posteriori* assessments based on actual LES simulations (Ma *et al*., 2013; Ma *et al*., 2014; Butz *et al*., 2015; Langella *et al*., 2017). Furthermore, it has been demonstrated earlier (Chakraborty and Cant, 2011; Chakraborty *et al*., 2014) that the wrinkling of these flames, is at least representative for some laboratory

flames (Muppala *et al*., 2005). The above aspects provide the confidence in the database itself and in the findings of the present analysis.

As this DNS database has been used many a time in the past, only a brief description of it has been provided here. A three-dimensional compressible code SENGA (Jenkins and Cant, 1999) is used where the mass, momentum, energy and reaction progress variable conservation equations are solved in non-dimensional form. A simple one-step Arrhenius-type chemistry has been used to keep the computational cost within reasonable limits. For the current analysis, the heat release parameter, $\tau = (T_{ad} - T_u)/T_u = 4.5$, and the Zel'dovich number, $\beta = T_{ac}(T_{ad} - T_u)/T_{ad}^2 = 6.0$ are taken, where the subscripts 'u' and 'b' indicate variables in the unburned and the burnt gases, and T_{ad}, T_u, and T_{ac} are the adiabatic flame, the unburned gas, and the activation temperatures, respectively. For hydrogen and hydrocarbon-air flames the Zel'dovich number β for global mechanisms varies between 6.0 to 8.0 (Poinsot and Veynante, 2001), whereas the heat release parameter τ depends on the extent of preheating (i.e. on the unburened gas temperature T_u). The values of β and τ used here are consistent with several previous analyses (Haworth and Poinsot, 1992; Rutland and Trouvé, 1993; Trouvé and Poinsot, 1994). It can be stated that the unity Lewis number flames are analogous to the stoichiometric methane-air flame, whereas the Lewis number 0.34 case is representative of a lean hydrogen-air mixture of an equivalence ratio of 0.3. The Lewis number 0.6 and 0.8 cases are representative of hydrogen-blended methane-air mixtures (e.g. 20% and 10% (by volume) hydrogen-blended methane-air flames with an overall equivalence ratio of 0.6) and the Lewis number 1.2 case is representative of a hydrocarbon-air mixture involving a hydrocarbon fuel which is heavier than methane (e.g. ethylene-air mixture with an equivalence ratio of 0.7) (Kobayashi *et al*.,1996; Law and Kwon, 2004; Muppala *et al*., 2005; Dinkelacker *et al*., 2011). Furthermore, the range of Lewis number considered here is comparable to that considered by

Trouvé and Poinsot (1994). The reaction progress variable c is defined based on the reactant mass fraction Y_R:

$$c = \frac{Y_{Ru} - Y_R}{Y_{Ru} - Y_{Rb}}, \tag{15}$$

The simulations have been conducted for five different values of global Lewis number *Le* (i.e., *Le* =0.34, 0.6, 0.8, 1.0 and 1.2) and, in every case, the domain has been taken to be a cube with all sides equal to $24.1\delta_{th}$, where $\delta_{th} = (T_{ad} - T_u)/\max|\nabla T|_L$ is the thermal flame thickness with *T* being the instantaneous dimensional temperature and the subscript '*L*' referring to the unstrained laminar flame quantity. The domain is discretised using a uniform Cartesian grid of 230 × 230 × 230, which ensures about 10 grid points within δ_{th}.

A planar laminar flame, used as the initial condition for the species field, interacts with a turbulent field, which has been initialised using a pre-computed incompressible homogeneous isotropic turbulence field (Rogallo, 1981). The domain is considered to be periodic in *y* and *z* directions, while partially non-reflecting boundary conditions are imposed in the *x* direction, using the Navier-Stokes Characteristic Boundary Conditions (NSCBC) approach (Poinsot and Lele, 1992). The spatial derivatives for the internal grid points are evaluated using a tenth-order central difference scheme and the order of differentiation drops gradually to a one-sided second-order scheme at the non-periodic boundaries. A third order explicit Runge-Kutta scheme (Wray, 1990) is used for time advancement.

The initial velocity and length scale ratios of every simulation have been taken to be $u'/S_L = 7.5$ and $l/\delta_{th} = 2.45$, respectively, which yield a Damköhler number $Da = (l/\delta_{th})/(u'/S_L) = 0.32$, and a Karlovitz number $Ka = (u'/S_L)^{3/2}(l/\delta_{th})^{-1/2} = 13.12$. The turbulent Reynolds number $Re_t = \rho_0 u' l/\mu_0$ is equal to 47 for all cases considered here where ρ_0, μ_0 and l are the unburned gas density, unburned gas viscosity and longitudinal integral length scale

respectively. One obtains an initial turbulent Reynolds number of about 70 if the integral length scale based on turbulent kinetic energy and its dissipation rate (i.e. $l_k = k^{1.5}/\varepsilon$) is considered. The turbulence has been allowed to interact with the laminar planar flame about 3.34 initial integral eddy turnover times (i.e. $3.34t_e = 3.34l/u'$), which amounts to one chemical time scale (i.e., δ_{th}/S_L) for the present thermo-chemistry. However, qualitative nature of all the results shown in this paper does not change for $t \geq 2l/u'$.This simulation time remains comparable to those of several previous analyses, which contributed significantly to the fundamental understanding of turbulent premixed combustion (Peters *et al*., 1998; Echekki and Chen, 1999; Ashurst *et al*., 1988; Haworth and Poinsot, 1992; Rutland and Trouvé, 1993; Trouvé and Poinsot, 1994; Boger *et al*., 1998; Pera *et al*., 2013).The velocity ratio decayed by 50% ahead of the flame, whereas the length ratio increased by a factor of 1.7 (which corresponds to $Da = (l/\delta_{th})/(u'/S_L) = 1.11$ and $Ka = (u'/S_L)^{3/2}(l/\delta_{th})^{-1/2} = 3.56$ The combustion nominally takes place in the 'thickened-wrinkled flame' regime (where flamelet assumption is expected to be valid) for all cases considered here (Peters, 2000). A range of Karlovitz number given by $1 < Ka < 10$ belongs to the flamelet regime of combustion which is realised in Internal Combustion (IC) engines and gas turbines (Poinsot and Veynante, 2001).

4. RESULTS & DISCUSSION

The distributions of non-dimensional temperature $\theta = (T - T_u)/(T_{ad} - T_u)$ at the central mid-plane in $x - y$ direction are shown in Fig. 1 when the statistics were extracted. The contours of $c = 0.1 - 0.9$ (in steps of 0.1 from left to right) are also shown by white lines. Figure 1 shows that the extent of flame wrinkling increases with decreasing Le, which can be quantified by the values of normalised flame surface area A_T/A_L (where flame surface area A is evaluated using the volume integral of $|\nabla c|$ as: $\int_V |\nabla c| dV = \sum \frac{\Delta c}{\Delta x_N} \Delta x_N A = \sum(\Delta c)A$ and the subscripts T and L are used for turbulent and laminar flames respectively) listed in Table 1. The greater

extent of flame wrinkling for smaller values of Le is consistent with previous findings (Sivashinsky, 1977; Clavin and Williams, 1982; Abdel-Gayed *et al*., 1984; Ashurst *et al*., 1988; Haworth and Poinsot, 1992; Rutland and Trouvé, 1993; Trouvé and Poinsot, 1994; Han and Huh, 2008; Muppala *et al*., 2005). This is a result of stronger focusing of reactants than the defocusing of heat at the flame wrinkles which are convex towards the reactants for $Le < 1$ flames, which leads to simultaneous occurance of high temperature and reactant concentration, and this tendency strengthens with decreasing Lewis number. This behaviour can be substantiated from Fig. 1, which shows that high temperature zones in the $Le < 1$ flames are associated with the wrinkles which are convex towards the reactants, and temperature values can be super-adiabatic (i.e. $\theta > 1$) in these regions for the $Le = 0.34$,0.6 and 0.8 cases. By contrast, a combination of strong focusing of heat and weak defocusing of reactants leads to high temperature values at the regions where the flame is concave to the reactants in the $Le = 1.2$ flame. The reaction progress variable c remains equal to θ for low Mach number adiabatic unity Lewis number flames as in the present $Le = 1.0$ case.

It is worth noting that the contours of c are more tightly packed on the burned gas sides of the flame than the contours on the unburned gas side of the flame in the $Le = 0.8$,1.0 and 1.2 cases considered here. The cases considered here nominally represent the thin reaction zones regime combustion (Peters, 2000), and thus energetic eddies enter into the preheat zone and perturb it, and this contributes to local thickening of the flame towards the unburned gas side. By contrast, in can be seen from Fig. 1 that the contours of c in the burned gas side for the $Le = 0.34$ and 0.6 cases are not as tightly packed towards the burned gas side as in the $Le = 0.8, 1.0$ and 1.2 cases and the flames in the $Le = 0.34$ and 0.6 cases exhibit considerable local thickening on the burned gas side, and this tendency strengthens with decreasing Le.

The larger extent of flame wrinkling and the simultaneous presence of high temperature and reactant concentration pockets lead to increased rates of burning and flame normal acceleration with decreasing Lewis number. This can be verified from the mean values of $\rho\dot{\omega}_c \times \delta_{th}/\rho_0 S_L$ conditional on c in Fig. 2 for the cases considered here. It can be seen from Fig. 2 that the magnitude of $\rho\dot{\omega}_c$ increases with decreasing Le. The augmentation of burning rate with decreasing Le can be quantified from the values of Ω_T/Ω_L listed in Table 1 where $\Omega = \int_V \rho\dot{\omega}_c dV$ is the volume integrated reaction rate. It can be seen from Table 1 that Ω_T/Ω_L remains close to A_T/A_L for flames with $Le = 1.0$ but the simultaneous occurrence of high reactant concentration and high temperature in the positively stretched zones leads to a much greater burning rate per unity area for $Le < 1$ flames, and this tendency strengthens with decreasing Le. This leads to $\Omega_T/\Omega_L \gg A_T/A_L$ in the $Le = 0.34$ and 0.6 flames considered here. The thermal diffusion stronger than the reactant mass diffusion into the positively stretched reaction zone leads to a reduction of burning rate per unity area for the $Le = 1.2$ case in comparison to that in the corresponding unity Lewis number case, which is responsible for $\Omega_T/\Omega_L < A_T/A_L$ in the $Le = 1.2$ case.

Recently, a number of studies conducted DNS of freely propagating fuel-lean turbulent premixed flames with different fuels with either detailed (Aspden *et al.*, 2011, 2015; Carlsson *et al.*, 2014; Aspden *et al.*, 2017) or reduced (Savard and Blanquart, 2015; Lapointe *et al.*, 2015) chemistry for different fuels (e.g. H_2, CH_4, propane, n-dodecane (in the increasing order of fuel Lewis number) by Aspden *et al.* (2017); H_2-air flames with equivalence ratios of 0.31 and 0.4 by Aspden *et al.* (2011, 2015) and n-Heptane by Savard and Blanquart (2015) and Lapointe *et al.* (2015)). These analyses also indicated that the overall burning rate quantified by volume-integrating reaction rate of the fuel (e.g. from n-dodecane to propne to CH_4 to H_2 in Aspden *et al.*, 2017) and heat release (e.g. higher heat release in H_2-air flame than the

corresponding CH_4-air flame) increase with decreasing Lewis number of the fuel. Furthermore, Savard and Blanquart (2015) and Lapointe *et al.* (2015) demonstrated that unity Lewis number assumption leads to an overestimation of the overall burning rate of lean n-heptane flames with characteristic Lewis number greater than unity (i.e. $Le > 1$). These findings are also in qualitative agreement with the variation of Ω_T/Ω_L with Le shown in Table 1 based on current simple chemistry results. It has been discussed in Chakraborty and Cant (2011) that the variation of A_T/A_L in response to Le in Table 1 is also consistent with experimental observations by Muppala *et al*. (2005).

It is worth noting that $\Omega_T/\Omega_L > A_T/A_L$ and super-adiabatic temperatures at positively curved zones for the $Le < 1$ flames (see Fig. 1) are indicative of thermo-diffusive instability in these flames and are the manifestation of this instability is stronger for smaller values of Le. It is worth noting that these effects of thermo-diffusive instability were also observed by detailed chemistry DNS results by Aspden *et al.* (2011) and Aspden *et al*. (2015) but these effects are somewhat masked by turbulence for large values of Ka but the effects of preferential diffusion due to non-unity Lewis number survive even for very large values of Ka. The augmentation of burning rate with decreasing Le is particularly prevalent for small values of Lewis number (i.e. $Le \ll 1$ and for example $Le = 0.34$ case considered here), which acts to increase the magnitude of positive dilatation rate $\nabla.\boldsymbol{u}$ (Chakraborty and Cant, 2009) and mean flame displacement speed S_d (Chakraborty and Cant, 2005) and also affects the alignment of ∇c with local principal strain rates (Chakraborty *et al*. 2009), and these aspects will be discussed later in detail in this section.

As the effective tangential and normal strain rates govern the evolutions of A and $|\nabla c|$, respectively, and the flame surface area A is somehow related to $|\nabla c|$, it is instructive to

understand the behaviour of the gradient of reaction progress variable across the flame front. The magnitude of the gradient of the reaction progress variable can be related to the distance between to prescribed iso-scalar surfaces, Δx_N, through the concept of the surface density function (Vervish *et al*., 1995), $\Sigma(\Gamma;\mathbf{x},t) = |\nabla c|\delta[\Gamma - c(\mathbf{x},t)]$. From our previous definitions $\Sigma(\Gamma;\mathbf{x},t) = \mathrm{A}(\mathbf{x},\mathrm{t})/\mathrm{V}(\mathbf{x},\mathrm{t}) = 1/\Delta x_N$, and, then, $1/|\nabla c| = \Delta x_N \delta[\Gamma - c(\mathbf{x},t)]$; conditional average of thes las relation yields $\langle 1/|\nabla c| \mid c(\mathbf{x},t) = \Gamma\rangle = \langle \Delta x_N \mid c(\mathbf{x},t) = \Gamma\rangle\, P_c(\Gamma;\mathbf{x},t)$, where $\langle 1/|\nabla c| \mid c(\mathbf{x},t) = \Gamma\rangle$ and $\langle \Delta x_N \mid c(\mathbf{x},t) = \Gamma\rangle$ are the mean values of $1/|\nabla c|$ and Δx_N conditional on $c(\mathbf{x},t) = \Gamma$, and $P_c(\Gamma;\mathbf{x},t)$ is the probability density function (PDF) of $c(\mathbf{x},t)$. The physical distance between two iso-surfaces $c(\mathbf{x},t) = c_\mathrm{m}$ and $c(\mathbf{x},t) = c_M$ is given by $\int_{c_m}^{c_M}\langle 1/|\nabla c| \mid c(\mathbf{x},t) = \Gamma\rangle\, d\Gamma = \int_{c_m}^{c_M}\langle \Delta x_N \mid c(\mathbf{x},t) = \Gamma\rangle\, P_c(\Gamma;\mathbf{x},t)\; d\Gamma$.

Figure 3a shows the variation of the mean values of $|\nabla c| \times \delta_L$ conditional on c, where δ_L is an alternative flame thickness which is defined as: $\delta_L = 1/\max|\nabla c|_L$ for an unstrained laminar flame. It can be seen from Fig. 3a that the peak of conditional mean values of $|\nabla c| \times \delta_L$ is greater than 1 for $Le = 0.34$, 0.6 and 0.8, whereas they remain smaller than 1.0 for the $Le = 1.2$ cases. In the $Le = 1.0$ case, the peak mean value of $|\nabla c| \times \delta_L$ conditional on c remains about unity. A peak conditional mean value of $|\nabla c| \times \delta_L = |\nabla c|/|\nabla c|_L > 1$ suggests that the flame front under turbulent condition becomes thinner than the laminar flame in a mean sense. By contrast, a peak conditional mean value of $|\nabla c| \times \delta_L = |\nabla c|/|\nabla c|_L < 1$ indicates a flame front thickening under turbulent condition in a mean sense, whereas the peak conditional mean value of $|\nabla c| \times \delta_L = |\nabla c|/|\nabla c|_L \approx 1$ suggests that the flame front thickness remains unaffected under the turbulent condition. It is yet to be ascertained whether the flame front thickens or becomes thinner through its interaction with a turbulent flow. Some existing experimental (Soika *et al*., 1998) and computational (Hawkes and Chen, 2006) data reported flame thinning under turbulence, whereas some other experimental (O'Young and Bilger,

1997; Chen and Mansour, 1998; Chen and Bilger, 2002) and computational (Sankaran *et al*., 2007; Moreau *et al*., 2011) analyses reported flame front thickening. In the current analysis, flame front thickening is found for the $Le > 1$ case, whereas flame front thinning has been found for $Le < 1$ cases.

The variations of $|\nabla c|/|\nabla c|_{max}$ conditional on c for both laminar and turbulent flames are shown in Figs. 3b-f for $Le = 0.34, 0.6, 0.8, 1.0$ and 1.2 respectively, where $|\nabla c|_{max}$ represents the peak mean value of $|\nabla c|$ conditional upon c. The quantity $|\nabla c|/|\nabla c|_{max}$ provides the relative magnitudes and thus a measure of relative thicknesses of different zones within the flame front. It is evident from Figs. 3b-f that there is a considerable difference between $|\nabla c|/|\nabla c|_{max}$ distributions between laminar and turbulent flames for the $Le = 0.34$ flame. This difference decreases with increasing Le and there is not much difference between the profiles for laminar and turbulent flames for $Le = 1.0$ and 1.2 cases. A higher (smaller) value of $|\nabla c|/|\nabla c|_{max}$ in a region of a turbulent flame, in comparison to the corresponding laminar value, indicates relative thinning (broadening) of the turbulent flame zone in consideration with respect to the overall flame thickness. It is clear from Figs. 3b-d that the relative width of the preheat (reaction zone) zone in comparison to the overall flame thickness shortens (widens) in $Le < 1$ cases and this tendency strengthens with decreasing Le. This is consistent with the local broadening of the flame towards the burned gas side for the $Le = 0.34$ case, as observed in Fig. 1. It is worth noting that the burning rate dependence on local curvature due to thermo-diffusive effects (e.g. high rate of burning at positively curved regions for $Le < 1$) also contributes to the flame front thinning/thickening in addition to the turbulent stretch effects but these effects are not straightforward to isolate in turbulent flames. Interested readers are referred to Chakraborty and Klein (2008) and Katragadda and Chakraborty (2012) for local curvature dependence of $|\nabla c|$ for the cases considered here.

To understand the observed $|\nabla c|$ behaviour, it is necessary to analyse the variations of displacement speed S_d and its components S_n, S_t and S_r across the flame front. The variations of the mean values of S_d/S_L, S_r/S_L, S_n/S_L, $(S_r + S_n)/S_L$ and S_t/S_L conditional on c are shown in Fig. 4. It can be seen from Fig. 4 that the mean value of S_d/S_L increases from the unburned reactants to the burned gas side for all cases due to density variation. The mean value of S_d/S_L increases with decreasing Le. To comprehend these trends, the variations of the components of S_r/S_L, S_n/S_L and S_t/S_L conditional on c need to be considered. It is evident from Fig. 4 that S_r/S_L assumes positive value throughout the flame and its magnitude increases with decreasing Le. It has already been shown that both $\rho\dot{\omega}_c \geq 0$ and $|\nabla c| = -\partial c/\partial x_N \geq 0$ increase with decreasing Le, but the increase in $\rho\dot{\omega}_c$ dominates over the increase in $|\nabla c|$ to result in an increasing trend of S_r/S_L with a decrease in global Lewis number Le. The mean normal diffusion component of displacement speed assumes small positive values towards the unburned gas side and large negative values on the burned gas side because of the similar qualitative behaviour of the flame normal molecular diffusion rate $(1/\rho)\{\partial[\rho D(\partial c/\partial x_N)]/\partial x_N\}$. It can be seen from Fig. 4c that the magnitude of the negative value of S_n/S_L increases with decreasing Le. The normal diffusion rate $(1/\rho)\{\partial[\rho D(\partial c/\partial x_N)]/\partial x_N\}$ can be expressed as $D(\partial^2 c/\partial x_N^2)$ if the spatial variations of ρD are ignored. This leads to $(1/\rho)\{\partial[\rho D(\partial c/\partial x_N)]/\partial x_N\}/|\nabla c| = -D(\partial^2 c/\partial x_N^2)/(\partial c/\partial x_N)$. Both $D, |\partial^2 c/\partial x_N^2|$ and $|\nabla c| = -(\partial c/\partial x_N) \geq 0$ increase with decreasing Le and the product of the first two variables (i.e. $|D(\partial^2 c/\partial x_N^2)|$) grows faster than the third one (i.e. $|\nabla c|$). A representative local normal profile of $c(x_N, t)$ depicts $(\partial^2 c/\partial x_N^2)$ varying from positive to negative values as c increases across the flame, which explains the sign shift of S_n.

It can be seen from Fig. 4 that the normalised combined reaction and normal diffusion component of displacement speed $(S_r + S_n)/S_L$ remains positive for all cases and grows with c. The mean contribution of S_t/S_L remains negligible for the $Le = 1.0$ and 1.2 flames but becomes increasingly negative with decreasing Le for $Le < 1$ cases. It is worth noting that all the flames considered here are statistically planar, which indicates that the contribution of mean k_m conditional on c remains negligible (not shown here but the magnitude of the mean value of $k_m \times \delta_{th}$ remains smaller than 0.01) throughout the flame. It can be seen from Fig. 1 that high temperature regions in the $Le < 1$ flames are associated with positive curvature and thus thermal diffusivity values are likely to be high in the positively curved regions of these flames. By contrast, high temperature and high thermal diffusivity regions are associated with negatively curved regions in the $Le > 1$ case, whereas the mass diffusivity D remains constant for a given value of c for the unity Lewis number case. The non-dimensional temperature θ and curvature k_m are indeed positively (negatively) correlated for $Le < 1$ ($Le > 1$) cases and this positive correlation for $Le < 1$ flames strengthens with decreasing Lewis number Le. The correlations between θ and k_m have been discussed elsewhere (Rutland and Trouvé, 1993; Chakraborty and Cant, 2005b; Chakraborty and Klein, 2008) in detail and thus are not discussed here.

A positive (negative) correlation between D and k_m for $Le < 1$ ($Le > 1$) flames leads to a situation whereby the mean value of $Dk_m = -S_t/2$ is expected to be greater (smaller) than the product of mean values of D and k_m according to the definition of the correlation coefficient. As the mean value of k_m is almost zero, the mean value of $Dk_m = -S_t/2$ is expected to be positive (negative) for $Le \ll 1$ ($Le > 1$) flames. Thus, the mean value of $S_t/S_L = -2Dk_m/S_L$ becomes increasingly negative with decreasing Le for $Le < 1$ flames, whereas the mean $S_t/S_L = -2Dk_m/S_L$ assumes positive values in the $Le = 1.2$ case. As D does not vary on a

given c-isosurface for $Le = 1.0$ flames, the mean value of $Dk_m = -S_t/2$ is close to zero for statistically planar $Le = 1.0$ flames due to vanishingly small mean k_m values. Thus the non-negligible mean values of S_t/S_L in non-unity Lewis number flames are outcomes of the non-linear curvature dependence of k_m. Figure 4 demonstrates that the high values of positive mean contribution of $(S_r + S_n)/S_L$ for small values of Le is principally responsible for high mean values of S_d/S_L.

Figure 5 shows the mean values of normalised flow volumetric dilatation rate, $\nabla \cdot \boldsymbol{u}$, the flow normal strain rate, a_N , the flow tangential strain rate, a_T, for all cases considered here. The mean value of flow volumetric dilatation rate $\nabla \cdot \boldsymbol{u}$ remains positive, accounting for the thermal expansion due to the chemical heat release. It has already been shown in Fig. 2 that the reaction rate $\rho\dot{\omega}_c$ increases with decreasing Le, which leads to higher heat release rate for flames with smaller values of Lewis number. Thus, the effects of thermal expansion and flame normal acceleration strengthen with decreasing Lewis number, which is reflected in an increasing trend of , $\nabla \cdot \boldsymbol{u}$ with a decrease in Le.

The mean flow normal strain rate, a_N , exhibits mostly positive values within the flame front but assumes weak negative values towards the unburned gas side of the flame. The scalar gradient, ∇c, in these cases shows predominant collinear alignment with the most extensive principal strain rate within the flame front, whereas this alignment changes to the eigen direction corresponding to the most compressive principal strain rate where the effects of heat release are weak (Chakraborty and Swaminathan , 2007; Chakraborty *et al*., 2009). Thus, $a_N = (e_\alpha \cos^2\alpha + e_\beta \cos^2\beta + e_\gamma \cos^2\gamma)$ (where e_α, e_β and e_γ are the most extensive, intermediate and most compressive principal strain rates and α, β and γ are, respectively, the angles of the associated eigenvectors with ∇c) assumes positive value within the flame but becomes negative

where ∇c aligns with the most compressive principal strain rate. The maximum mean value of a_N is reached slightly towards the burned gas side ($c \approx 0.72$) of the flame front. Therefore, the flow normal strain rate tends to separate two adjacent iso-scalar surfaces, $c(\mathbf{x}, t) = \Gamma$ and $c(\mathbf{x}, t) = \Gamma + \Delta\Gamma$, pulling them apart, within the flame region. The stronger flame normal acceleration along with the collinear alignment between ∇c and e_α contribute an increase in the positive mean value of a_N with decreasing Lewis number.

The relative balances between $\nabla \cdot \boldsymbol{u}$ and a_N determine the behaviour of tangential strain rate $a_T = \nabla \cdot \boldsymbol{u} - a_N$. The mean tangential strain rate a_T remains positive for all values of c for all cases considered here. Apart from the Le = 0.34 case, the remaining cases display similar trends with an almost constant value across the flame front. For the Le = 0.34 case, the mean value of a_T increases with c from the unburned gas side and attains a peak value before decreasing gradually towards the burned gas side.

Here, the flow strain rate tangential to the iso-surfaces has been found to be smaller, though not negligible, in comparison to that in the normal direction. This is a consequence of the volumetric dilatation rate in a given topology of iso-scalar surfaces embedded in the flame. The relative magnitudes of $\nabla . \boldsymbol{u}$ and a_N determine the magnitude of a_T. For high-Ka flames, the scalar gradient ∇c preferentially aligns with the most compressive principal strain rate (which is not the cases considered here) and thus mean a_N assumes negative value, whereas $\nabla . \boldsymbol{u}$ is expected to weak due to the disturbances in the reaction zone for these flames. As a result, in high-Ka flames (where $\nabla . \boldsymbol{u} \ll a_T$ and $a_T \approx -a_N$), the magnitude of the mean value of a_T is expected to comparable to that of a_N.

The mean contributions of the added normal strain rate due to flame propagation $\partial S_d/\partial x_N$ conditional on c along with its components (i.e. $\partial S_r/\partial x_N$, $\partial S_n/\partial x_N$ and $\partial S_t/\partial x_N$) are shown in Fig. 6. It can be seen from Fig. 6 that the mean contribution of $\partial S_d/\partial x_N$ conditional on c remains mostly negative for all Lewis numbers and in the $Le = 0.34$ case the mean value of $\partial S_d/\partial x_N$ assumes positive values both on unburned and burned gas sides of the flame front. The mean contributions of $\partial S_r/\partial x_N$ remain negative throughout the flame which is consistent with the behaviour of S_r (depicted in Fig. 4b), which increases from the unburned to the burned gas side of the flame (i.e., in the direction opposite to the flame normal); derivative of S_r yields $\partial S_r/\partial x_N = -(\partial \dot{\omega}_c/\partial c) + [\dot{\omega}_c/(\partial c/\partial x_N)^2](\partial^2 c/\partial x_N^2)$, which indicate that the two terms of this expression lead to a negative $\partial S_r/\partial x_N$ for c > 0.6. The mean contribution of $\partial S_n/\partial x_N$ assumes small (large) negative (positive) values on the unburned (burned) gas side of the flame front due to predominantly positive (negative) values of S_n (see Fig. 4). The increase in the magnitude of predominantly negative values of S_t from the unburned to burned gas side of the flame for $Le < 1$ cases leads to a positive mean contribution of $\partial S_t/\partial x_N$ and this mean value increases with decreasing Le. The mean contribution of $\partial S_t/\partial x_N$ remain negligible for the $Le = 1.0$ case and this contribution for $Le = 1.2$ remains weakly negative. The combination of high magnitudes of S_r, S_n and ∇c (see Figs. 3 and 4) for small Lewis number flames leads to an increase in the magnitudes of $\partial S_r/\partial x_N$ and $\partial S_n/\partial x_N$ with a decrease in Le. The relative magnitudes of the mean contributions of $\partial S_r/\partial x_N$, $\partial S_n/\partial x_N$ and $\partial S_t/\partial x_N$ determine the magnitude of the mean value of $\partial S_d/\partial x_N$. The magnitude of the mean value of $\partial S_d/\partial x_N$ increases with decreasing Le.

The normalised mean values of the added tangential strain rate (or the curvature stretch term), $2k_m S_d$, conditional on c for the cases considered here are presented in Fig. 7, which shows

negative mean values of $2k_mS_d$ throughout the flame for all cases considered here. In order to understand this behaviour, it is useful to split $2k_mS_d$ in the following manner:

$$2k_mS_d = 2k_m(S_r + S_n + S_t) = 2k_m(S_r + S_n) - 4Dk_m^2 \quad (15)$$

The variations of normalised mean values of $2k_m(S_r + S_n)$ and $-4Dk_m^2$ conditional on c for all cases considered here are also shown in Fig. 7. It can be seen from Fig. 7 that the mean contribution of $-4Dk_m^2$ remains negative but its magnitude increases with decreasing Le due to a combination of high extent of flame wrinkling (which gives rise to the increased probability of obtaining high values of k_m^2) and high diffusivity D values for small values of Lewis number Le. Figure 7 further shows that positive mean values of $2k_m(S_r + S_n)$ are obtained for $Le < 1$, and its magnitude increases with decreasing Lewis number. By contrast, weak negative mean values of $2k_m(S_r + S_n)$ are obtained for the $Le = 1.2$ case, whereas the mean value of $2k_m(S_r + S_n)$ remains negligible for the unity Lewis number case. The observed behaviour of $2k_m(S_r + S_n)$ in statistically planar flames (where mean k_m is close to zero) originates due to the positive correlation between $(S_r + S_n)$ and k_m in $Le < 1$ flames, whereas a negative correlation is obtained for $Le > 1$ flames (see Fig. 4 in Katragadda and Chakraborty, 2012). These quantities (i.e., $(S_r + S_n)$ and k_m) are weakly correlated for the unity Lewis number flames. The physical explanations for the aforementioned correlations between $(S_r + S_n)$ and k_m have been explained elsewhere (Chakraborty and Cant, 2005b; Chakraborty and Klein, 2008), and thus are not repeated here. The mean negative contribution of $-4Dk_m^2$ dominates over the mean value of $2k_m(S_r + S_n)$ throughout the flame to give rise to a net negative mean value of $2k_mS_d$ for all cases considered here.

The variations of the normalised mean values of a_N^{eff} conditional on c for all cases are shown in Fig. 8a, which shows that mean effective normal strain rate remains positive for all cases

considered here. The relative magnitudes of the mean values of a_N and $\partial S_d/\partial x_N$ determines the mean value of a_N^{eff}. A comparison between Figs. 5 and 6 reveals that the positive mean value of a_N dominates over mostly negative mean values of $\partial S_d/\partial x_N$ to yield positive mean values of a_N^{eff}. It is worth noting that flame-turbulence interaction takes place under decaying turbulence for the cases considered here, and thus the variation of a_N^{eff} is not sufficient to infer about the evolution of $|\nabla c|$ and in these cases. As in these cases the inlet velocity is not adjusted to match the turbulent flame speed, the mean contribution of $\{v_j^c(\partial|\nabla c|/\partial x_j)\}|\nabla c|^{-1} = \{(u_j + S_d N_j)(\partial|\nabla c|/\partial x_j)\}|\nabla c|^{-1}$ in Eq. (13) is expected to be mostly negative except towards the burned gas side of the flame front. This can be substantiated from the variation of the mean contribution of $\{(u_j + S_d N_j)(\partial|\nabla c|/\partial x_j)\}|\nabla c|^{-1}$ shown in Fig. 8b for all cases considered here. The magnitudes of $\{(u_j + S_d N_j)(\partial|\nabla c|/\partial x_j)\}|\nabla c|^{-1}$ and a_N^{eff} determine the mean behaviour of $\{\partial|\nabla c|/\partial t\}|\nabla c|^{-1}$.[1] It can be seen from Fig. 8c that the negative contributions of $\{(u_j + S_d N_j)(\partial|\nabla c|/\partial x_j)\}|\nabla c|^{-1}$ dominate over positive a_N^{eff} values to yield strong mean positive values of $\{\partial|\nabla c|/\partial t\}|\nabla c|^{-1}$ over a significant fraction of the flame thickness before the mean values of $\{\partial|\nabla c|/\partial t\}|\nabla c|^{-1}$ become negative towards the burned gas side in the $Le = 0.34$ and 0.6 cases (with an increasing magnitude with decreasing Le). The negative (positive) mean value of $\{\partial|\nabla c|/\partial t\}|\nabla c|^{-1}$ on the burned (unburned) gas side is indicative of an increase (a decrease) of the relative width of the reaction zone (preheat zone) in the $Le = 0.34$ and 0.6 cases, which is consistent with the observations made from Fig.1 regarding broadening the gap between c contours towards the burned gas side of the flame front. The mean value $\{\partial|\nabla c|/\partial t\}|\nabla c|^{-1}$ remains small for the $Le = 0.8, 1.0$ and 1.2 cases with decreasing magnitude with an increase in Le.

[1] The agreement of transient term of the $|\nabla c|$ transport equation evaluated from the transport equation and the actual evaluation from two time snapshots has been found to be very good (i.e. maximum deviation is smaller than 2%).

The variation of mean values of the effective tangential strain rate of a_T^{eff} conditional on c is presented in Fig. 8d. For $Le = 0.34, 0.6$ and 0.8 the positive mean value of a_T dominates over the mostly negative mean contribution of $2k_m S_d$ to yield a positive mean value of a_T^{eff}, and the magnitude of a_T^{eff} increases with decreasing Le. The magnitude of the mean value of a_T^{eff} remains small for the major part of the flame and exhibits positive values towards the unburned gas side before assuming negative values towards the burned gas side for the $Le = 1.0$ and 1.2 cases. The positive mean value of a_T^{eff} throughout the flame with an increasing magnitude with a decrease in Le explains the greater extent of flame wrinkling for smaller values of Lewis number (see Fig. 1). The small negative mean values of a_T^{eff} for the $Le = 1.0$ and 1.2 cases are consistent with the stabilisation mechanism associated with Huygens propagation which suggests that a smooth perturbed flame surface will eventually form cusps and become flatter with time, and this is further augmented by the thermo-diffusive stablility in the $Le = 1.2$ case. This mean behaviour of a_T^{eff} in the $Le = 1.0$ and 1.2 cases provides the explanation why these flames are less wrinkled in comparison to the flames with $Le < 1$.

Finally, it is worth pointing out a physical interpretation of the added strain rates. For a non-material elementary volume, V, of varying mass $m_{NM} = \rho V$, time derivative leads to $(1/m_{NM})(dm_{NM}/dt) = (1/\rho)(d\rho/dt) + (1/V)(dV/dt)$. Eq. (9) can be used to replace the last term and obtain $(1/m_{NM})(dm_{NM}/dt) = (1/\rho)(d\rho/dt) + a_N + \frac{\partial S_d}{\partial x_N} + a_T + 2k_m S_d$, which finally simplifies to yield $(1/m_{NM})(dm_{NM}/dt) = (\partial S_d/\partial x_N) + 2k_m S_d$. Therefore, summation of the added normal and tangential strain rates provides an expression for the mass entrainment rate per unit mass into an elementary nonmaterial volume.

5. CONCLUSIONS

The influences of the Lewis number on the 'effective' strain rates and the evolution of the scalar gradient magnitude have been analysed using three-dimensional variable-density simple chemistry direct numerical simulations of freely propagating turbulent premixed flames representing nominally the 'thickened-wrinkled flame' regime with global Lewis numbers of $Le = 0.34, 0.6, 0.8, 1.0$ and 1.20. It has been found that the flame area generation increases with decreasing Le. Moreover, the thickness of the turbulent flame front becomes increasingly smaller than the laminar flame thickness in a mean sense with decreasing Le for sub-unity (i.e., $Le < 1$) Lewis number flames. By contrast, just the opposite behaviour (i.e., flame front thickening in comparison to the corresponding laminar flame) has been observed for the $Le = 1.2$ flame considered here. The statistics of the flow normal and tangential strain rates, volumetric dilatation rate, and the 'added' tangential and normal strain rates, conditional upon the progress variable have been investigated in detail. The statistical behaviour of dilation rate, $\nabla \cdot \boldsymbol{u}$, has been found to be significantly affected by Le, and the mean dilatation rate increases with decreasing Lewis number. The mean flow normal strain rate, a_N, follows the trends of $\nabla \cdot \boldsymbol{u}$ and is mostly positive within the flame. Surface stretching due to the flow tangential strain rate, a_T remains positive throughout the flame front. The mean 'added' tangential strain rate, $2S_d k_m$, assumes negative values throughout the flame due to the tangential diffusion component of displacement speed $S_t = -2Dk_m$. The negative contribution of $\partial S_r/\partial x_N$ arising due to chemical conversion dominate over the contributions due to the tangential diffusion and the normal diffusion components (i.e., $\partial S_n/\partial x_N$ and $\partial S_t/\partial x_N$) to give rise to predominantly negative values of $\partial S_d/\partial x_N$. The relative magnitudes of a_N and $\partial S_d/\partial x_N$ determine the mean behaviour of the effective normal strain rate a_N^{eff}, and similarly the mean behaviour of effective tangential strain rate a_T^{eff} is governed by the relative magnitudes of the mean values of a_T and $2S_d k_m$. The mean value of a_N^{eff} turns out to be mostly positive for all cases considered here

and its magnitude increases with decreasing Le. It has been found that the statistical behaviour of $\{(u_j + S_d N_j)(\partial|\nabla c|/\partial x_j)\}|\nabla c|^{-1}$ along with a_N^{eff} determine whether the flame front thickens or becomes thinner under flame-turbulence interaction. Both a_T^{eff} and a_N^{eff} statistics have been utilised to explain the flame front thinning (thickening) for $Le < 1$ ($Le > 1$) flames and the increasing trend of flame area generation with decreasing Le. Finally, in addition to the Lewis number, it is expected that the Karlovitz number will have a significant effect on the evolution of the scalar gradient magnitude in turbulent premixed flames. The Karlovitz number dependence of flow normal and tangential strain rates, volumetric dilatation rate, and the "added" tangential and normal strain rates will be addressed in future research.

ACKNOWLEDGEMENTS

C.D. and L.C. gratefully acknowledge the support of this research by the Spanish Ministry of Economy and Competitiveness, under the CONSOLIDER-INGENIO Program, Project CS D2010-00011-SCORE. NC acknowledges N8/ARCHER for computational resources.

REFERENCES

Abdel-Gayed, R.G., Bradley, D., Hamid, M., and Lawes, M. 1984. Lewis number effects on turbulent burning velocity, Proc. Combust. Inst., 20, 505.

Allauddin, U., Pfitzner, M., Klein, M., Chakraborty, N. 2017. A-priori and a-posteriori analysis of algebraic flame surface density modelling in the context of large eddy simulation of turbulent premixed combustion, Numer. Heat Trans. A., 71, 153.

Ashurst, W.T, Peters, N., and Smooke, M.D. 1988. Numerical simulation of turbulent flame structure with non-unity Lewis number, Combust. Sci. Technol., 53,339.

Aspden, A. J., Day, M.S., Bell, J.B. 2011. Turbulence–flame interactions in lean premixed hydrogen: transition to the distributed burning regime, J. Fluid Mech., 690, 287.

Aspden, A. J., Day, M.S., Bell, J.B. 2015. Turbulence-chemistry interaction in lean premixed hydrogen combustion, Proc. Combust. Inst., 35, 1321.

Aspden, A. J., Bell, J.B., Day, M.S., Egolfopoulos, F. 2017. Turbulence-Flame Interactions in Lean Premixed Dodecane Flames, Proc. Combust. Inst., 36, 2005.

Boger, M., Veynante, D., Boughanem, H., Trouvé, A. 1998. Direct Numerical Simulation analysis of flame surface density concept for Large Eddy Simulation of turbulent premixed combustion, Proc. Combust. Inst., 27, 917.

Butz, D., Gao, Y., Kempf, A.M., Chakraborty, N. 2015. Large Eddy Simulations of a turbulent premixed swirl flame using an algebraic Scalar Dissipation Rate closure, Combust. Flame, 162, 3180.

Candel, S.M., Poinsot, T.J. 1990. Flame stretch and the balance equation for the flame area, Combust. Sci. Technol., 70,1.

Carlsson, H., Yu, R., Bai, X-S. 2014. Direct numerical simulation of lean premixed CH4/air and H2/air flames at high Karlovitz numbers, Int. J. Hydrogen Energy, 39, 20216.

Chakraborty, N., Cant, R.S. 2005a. Effects of strain rate and curvature on Surface Density Function transport in turbulent premixed flames in the thin reaction zones regime, Phys. Fluids, 17, 65108.

Chakraborty, N., Cant, R.S. 2005b. Influence of Lewis Number on curvature effects in turbulent premixed flame propagation in the thin reaction zones regime, Phys. Fluids, 17,105105.

Chakraborty, N., Swaminathan, N. 2007. Influence of Damköhler number on turbulence-scalar interaction in premixed flames, Part I: Physical Insight, Phys. Fluids, 19, 045103.

Chakraborty, N., Klein, M. 2008. Influence of Lewis number on the Surface Density Function transport in the thin reaction zones regime for turbulent premixed flames, Phys. Fluids, 20, 065102.

Chakraborty, N., Hawkes, E.R., Chen, J.H., Cant, R.S. 2008. Effects of strain rate and curvature on Surface Density Function transport in turbulent premixed CH_4-air and H_2-air flames: A comparative study, Combust. Flame, 154,259.

Chakraborty, N., Klein, M., Swaminathan, N. 2009. Effects of Lewis number on reactive scalar gradient alignment with local strain rate in turbulent premixed flames, Proc. Combust. Inst., 32,1409.

Chakraborty, N., Cant, R.S. 2009. Effects of Lewis number on scalar transport in turbulent premixed flames, Phys. Fluids, 21, 035110.

Chakraborty, N., Swaminathan, N. 2010. Effects of Lewis number on scalar dissipation transport and its modelling implications for turbulent premixed combustion, Combust. Sci. Technol.,182, 1201.

Chakraborty, N., Cant, R.S. 2011. Effects of Lewis number on Flame Surface Density transport in turbulent premixed combustion, Combust. Flame, 158, 1768.

Chakraborty, N., Katragadda, M., Cant, R.S. 2011. Effects of Lewis number on turbulent kinetic energy transport in turbulent premixed combustion, Phys. Fluids, 23, 075109.

Chakraborty, N., Lipatnikov, A.N. 2013. Effects of Lewis number on the statistics of conditional fluid velocity in turbulent premixed combustion in the context of Reynolds Averaged Navier Stokes simulations, Phys. Fluids, 25, 045101.

Chakraborty, N., Wang, L., Klein, M. 2014. Effects of Lewis number on streamline segment analysis of turbulent premixed flames, Phys. Rev. E , 89, 033015, 2014.

Chakraborty, N., Konstantinou, I., Lipatnikov, A. 2016. Effects of Lewis number on vorticity and enstrophy transport in turbulent premixed flames, Phys. Fluids, 28,015109.

Chen, Y.-C., Monsour, M. S. 1998. Investigation of flame broadening in turbulent premixed flames in the thin reaction-zones .Combust. Inst., 27, 811.

Chen, Y.-C., Bilger, R. W. 2002. Experimental investigation of three-dimensional flame-front structure in premixed turbulent combustion-I: Hydrocarbon/air Bunsen flames, Combust. Flame, 131, 400.

Chung, S.H., Law, C.K. 1984. An Invariant Derivation of Flame Stretch.Combust. Flame, 55, 123-125.

Clavin P., and Williams, F.A. 1982. Effects of molecular diffusion and thermal expansion on the structure and dynamics of turbulent premixed flames in turbulent flows of large scale and small intensity, J.Fluid Mech., 128,251.

Cifuentes, L., Dopazo, C., Martin, J., Jimenez, C. 2014. Local flow topologies and scalar structures in a turbulent premixed flame, Phys. Fluids, 26, 065108.

Cifuentes, L., Dopazo, C., Martin, J., Domingo, P., Vervisch, L. 2015. Local volumetric dilatation rate and scalar geometries in a premixed methane-air turbulent jet flame, Proc. Comb. Inst., 35, 1295.

Dinkelacker , F., Manickam, B., Mupppala, S.R. 2011. Modelling and Simulation of lean premixed turbulent methane/hydrogen/air flames with an effective Lewis number approach, Combust. Flame, 158, 1742.

Dopazo, C., Cifuentes, L., Martin, J., Jimenez, C. 2015. Strain rates normal to approaching isoscalar surfaces in a turbulent premixed flame, Combust. Flame, 162, 1729.

Dopazo, C., Cifuentes, L., Hierro, J., Martin, J. 2015. Micro-scale mixing in turbulent constant density reacting flows and premixed combustion, Flow Turb. Comb., 96, 547.

Dopazo, C., Cifuentes, L. 2016. The physics of scalar gradients in turbulent premixed combustion and its relevance to modeling, Combust. Sci. Technol., 188, 1376.

Echekki, T., and Chen, J.H. 1999. Analysis of the Contribution of Curvature to Premixed Flame Propagation, Combust. Flame, 118, 303.

Gao, Y., Chakraborty, N., Swaminathan, N. 2014. Algebraic closure of Scalar Dissipation Rate for Large Eddy Simulations of turbulent premixed combustion, Combust. Sci. Technol., 186, 1309.

Gao, Y., Chakraborty, N., Klein, M. 2015. Assessment of the performances of sub-grid scalar flux models for premixed flames with different global Lewis numbers: A Direct Numerical Simulation analysis, Int. J. Heat Fluid Flow, 52, 28.

Han, I., Huh, K. 2008. Roles of displacement speed on evolution of flame surface density for different turbulent intensities and Lewis numbers in turbulent premixed combustion, Combust. Flame, 152, 194–205.

Hawkes, E. R., Chen, J. H. 2006. Comparison of direct numerical simulation of lean premixed methane–air flames with strained laminar flame calculations, Combust. Flame, 144, 112.

Haworth, D.C., and Poinsot, T.J. 1992. Numerical simulations of Lewis number effects in turbulent premixed flames, J. Fluid Mech., 244, 405.

Jenkins, K. W., Cant, R. S. 1999. DNS of turbulent flame kernels, in Proceedings of the Second AFOSR Conference on DNS and LES, Kluwer Academic, Dordrecht, 1999 (Eds. L. Sakell and T. Beautner), p. 192-202.

Katragadda, M., Chakraborty, N. 2012. A-priori Direct Numerical Simulation modelling of the curvature term of the Flame Surface Density transport equation for non-unity Lewis number flames in the context of Large Eddy Simulations, Int. J. Chem Engg., 2012, 103727.

Katragadda, M., Chakraborty, N., Cant, R.S. 2012. A-priori DNS assessment of wrinkling factor based algebraic Flame Surface Density models in the context of Large Eddy Simulations for non-unity Lewis number flames in the thin reaction zones regime, J. Combust., 794671.

Kim, S.H., Pitsch, H. 2007. Scalar gradient and small-scale structure in turbulent premixed combustion, Phys. Fluid 19,115104.

Klein, M., Chakraborty, N., Pfitzner, M. 2016. Analysis of the combined modelling of subgrid transport and filtered flame propagation for premixed turbulent combustion, Flow Turb. Combust., 96, 921.

Kobayashi, H., Tamura, H., Maruta, K., Nikola, T., Williams, F.A. 1996. Burning velocity of turbulent premixed flames in a high-pressure environment, Proc. Combust. Inst., 26, 389.

Kollmann, W., Chen, J.H. 1998. Pocket formation and the flame surface density equation, Proc. Combust. Inst., 27, 927.

Langella, I., Swaminathan, N., Gao, Y., Chakraborty, N. 2017. LES of premixed combustion using an algebraic closure involving scalar dissipation rate, Combust. Sci. Technol., 189, 43.

Lapointe, S., Savard, B., Blanquart, G. 2015. Differential diffusion effects, distributed burning, and local extinctions in high Karlovitz premixed flames, Combust. Flame, 162, 3341.

Law, C.K., Kwon, O.C. 2004. Effects of hydrocarbon substitution on atmospheric hydrogen–air flame propagation, Int. J. Hydrogen Energy, 29, 867.

Ma, T., Stein, O., Chakraborty, N., Kempf, A. 2013. A-posteriori testing of Algebraic Flame Surface Density models for LES, Combust. Theor. Model, 17, 431.

Ma, T., Gao, Y., Kempf, A., Chakraborty, N. 2014. Validation and Implementation of algebraic LES modelling of Scalar Dissipation Rate for reaction rate closure in turbulent premixed combustion, Combust. Flame, 161, 3134.

Moureau, V., Domingo, P., Vervisch, L. 2011. From Large-Eddy Simulation to Direct Numerical Simulation of a lean premixed swirl flame: Filtered laminar flame-PDF modeling, Combust. Flame, 158, 1340.

Muppala, S.P.R., Aluri, N.K., Dinkelacker, F., Leipertz, A. 2005. Development of an algebraic reaction rate closure for the numerical calculation of turbulent premixed methane, ethylene, and propane/air flames for pressures up to 1.0 MPa, Combust. Flame, 140, 257–266.

O'Young, F., Bilger, R. W. 1997. Scalar gradient and related quantities in turbulent premixed flames, Combust. Flame, 109, 683.

Pera, C., Chevillard, S., Reveillon, J. 2013. Effects of residual burnt gas heterogeneity on early flame propagation and on cyclic variability in spark-ignited engines, Combust. Flame, 160, 1020.

Peters, N. 2000. Turbulent Combustion, Cambridge Monograph on Mechanics, Cambridge University Press, Cambridge.

Peters, N., Terhoeven, P., Chen, J.H., and Echekki, T. 1998. Statistics of Flame Displacement Speeds from Computations of 2-D Unsteady Methane-Air Flames, Proc. Combust. Inst., 27,833.

Poinsot, T., Lele, S.K. 1992. Boundary conditions for direct simulation of compressible viscous flows, J. Comp. Phys., 101, 104.

Poinsot, T., Veynante, D. 2001. Theoretical and numerical combustion, R.T.Edwards Inc., Philadelphia, USA.

Pope, S.B. 1988. The evolution of surfaces in turbulence, Int J. Engng. Sci., 26, 445.

Rogallo, R.S. 1981. Numerical experiments in homogeneous turbulence, NASA Technical Memorandum 81315, NASA Ames Research Center, California.

Rutland, C., Trouvé, A. 1993. Direct Simulations of premixed turbulent flames with nonunity Lewis numbers, Combust. Flame, 94, 41.

Sankaran, R., Hawkes, E.R., Chen, J.H., Lu, T., Law, C.K. 2007. Structure of a spatially developing turbulent lean methane–air Bunsen flame, Proc. Combust. Inst. 31, 1291.

Savard, B, Blanquart, G. 2015. Broken reaction zone and differential diffusion effects in high Karlovitz n-C7H16 premixed turbulent flames, Combust. Flame, 162, 2020.

Sivashinsky, G.I. 1977. Diffusional-thermal theory of cellular flames, Combust. Sci. Technol., 16,137.

Soika, A., Dinkelacker, F., Leipertz, A. 1998. Measurement of resolved flame structure with constant Reynolds number, Proc. Comb. Inst., 27,785.

Trouvé, A., and Poinsot, T. 1994. The evolution equation for flame surface density in turbulent premixed combustion, J. Fluid Mech., 278, 1.

Vervisch, L., Bidaux, E., Bray, K.N.C., and Kollmann, W. 1995. Surface density function in premixed turbulent combustion modelling, similarities between probability density function and flame surface approaches, Phys. Fluids A, 7, 2496.

Veynante, D., Vervisch, L. 2002. Turbulent combustion modelling, Prog. Energy and Combust. Sci., 28, 193.

Wray, A.A. 1990. Minimal storage time advancement schemes for spectral methods, unpublished report, NASA Ames Research Center, California.

TABLES

Le	A_T/A_L	Ω_T/Ω_L
0.34	3.73	13.70
0.6	2.66	4.58
0.8	2.11	2.53
1.0	1.84	1.83
1.2	1.76	1.50

Table 1: Values of normalised flame surface area A_T/A_L and normalised burning rate Ω_T/Ω_L when statistics were extracted.

FIGURE CAPTIONS

Figure 1: Distribution of non-dimensional temperature θ in the central x-y plane for cases (a) $Le = 0.34$, (b) $Le = 0.6$, (c) $Le = 0.8$, (d) $Le = 1.0$ and (e) $Le = 1.2$ at the time statistics were extracted. The white lines show reaction progress variable c contours from 0.1 to 0.9 (from left to right) in steps of 0.1.

Figure 2: Variation of mean values of $\rho\dot{\omega}_c \times \delta_{th}/\rho_0 S_L$ conditional on c for all cases considered here.

Figure 3: Variation of mean values of $|\nabla c| \times \delta_L$ conditional on c for all cases considered here. The dotted line indicates $|\nabla c| \times \delta_L = 1.0$. Variation of the mean value of $|\nabla c|/|\nabla c|_{max}$ conditional on c for both laminar and turbulent cases (b) $Le = 0.34$, (c) $Le = 0.6$, (d) $Le = 0.8$, (e) $Le = 1.0$ and (f) $Le = 1.2$. Here $|\nabla c|_{max}$ refers to the maximum value of the mean value of $|\nabla c|$ conditional on c.

Figure 4: Variations of the mean values of (a) S_d/S_L, (b) S_r/S_L, (c) S_n/S_L, (d) $(S_r + S_n)/S_L$ and (e) S_t/S_L conditional on c for all cases considered here.

Figure 5: Variations of the mean values of (a) $\partial u_i/\partial x_i \times \delta_{th}/S_L$, (b) $a_N \times \delta_{th}/S_L$ and (c) $a_T \times \delta_{th}/S_L$conditional on c for all cases considered here.

Figure 6: Variations of the mean values of (a) $\partial S_d/\partial x_N \times \delta_{th}/S_L$, (b) $\partial S_r/\partial x_N \times \delta_{th}/S_L$, (c) $\partial S_n/\partial x_N \times \delta_{th}/S_L$ and (d) $\partial S_t/\partial x_N \times \delta_{th}/S_L$conditional on c for all cases considered here.

Figure 7: Variations of the mean values of (a) $2S_d k_m \times \delta_{th}/S_L$, (b) $2(S_r + S_n)k_m \times \delta_{th}/S_L$ and (c) $(-4Dk_m^2) \times \delta_{th}/S_L$conditional on c for all cases considered here.

Figure 8: Variations of the mean values of (a) $a_N^{eff} \times \delta_{th}/S_L$, (b) $\{(u_j + S_d N_j)\partial|\nabla c|/\partial x_j\}|\nabla c|^{-1} \times \delta_{th}/S_L$, (c) $\{\partial|\nabla c|/\partial t\}|\nabla c|^{-1} \times \delta_{th}/S_L$ and (d) $a_T^{eff} \times \delta_{th}/S_L$conditional on c for all cases considered here.

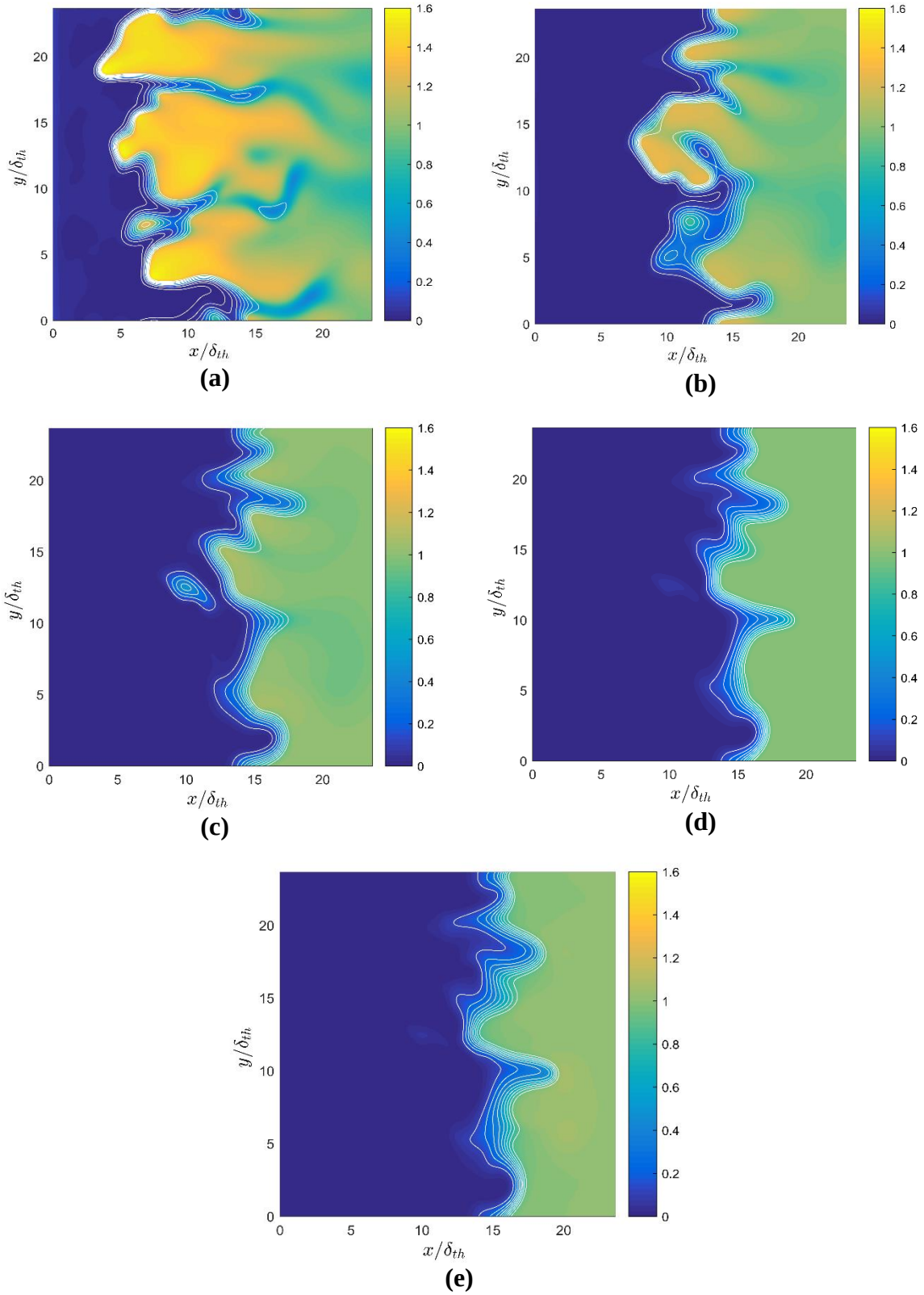

Figure 1: Distribution of non-dimensional temperature θ in the central *x-y* plane for cases (a) $Le = 0.34$, (b) $Le = 0.6$, (c) $Le = 0.8$, (d) $Le = 1.0$ and (e) $Le = 1.2$ at the time statistics were extracted. The white lines show reaction progress variable *c* contours from 0.1 to 0.9 (from left to right) in steps of 0.1.

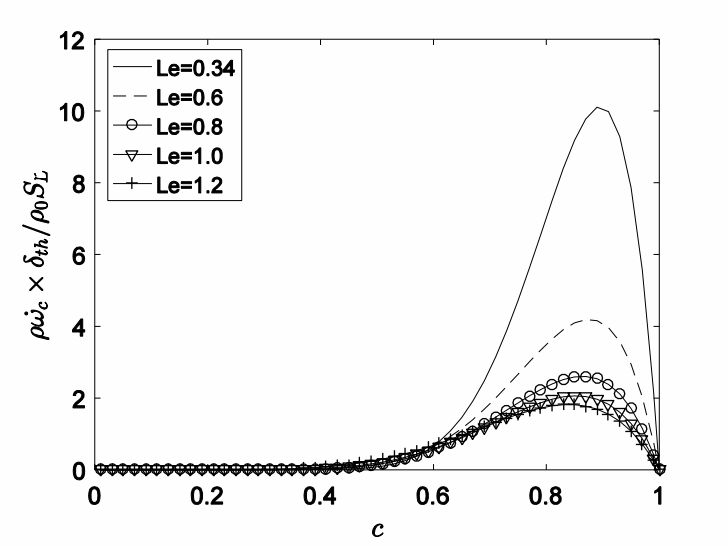

Figure 2: Variation of mean values of $\rho\dot{\omega}_c \times \delta_{th}/\rho_0 S_L$ conditional on c for all cases considered here.

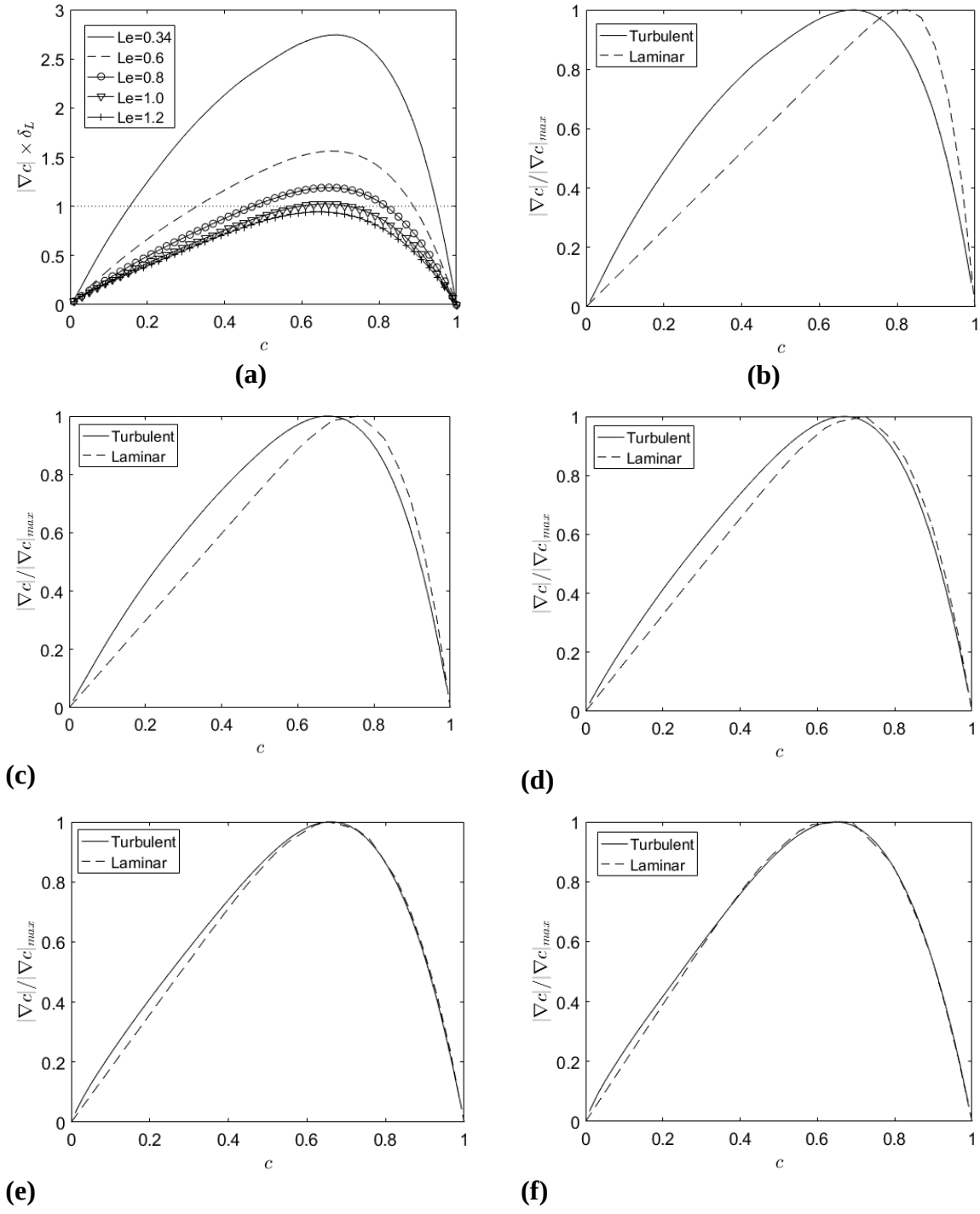

Figure 3: Variation of mean values of $|\nabla c| \times \delta_L$ conditional on c for all cases considered here. The dotted line indicates $|\nabla c| \times \delta_L = 1.0$. Variation of the mean value of $|\nabla c|/|\nabla c|_{max}$ conditional on c for both laminar and turbulent cases (b) $Le = 0.34$, (c) $Le = 0.6$, (d) $Le = 0.8$, (e) $Le = 1.0$ and (f) $Le = 1.2$. Here $|\nabla c|_{max}$ refers to the maximum value of the mean value of $|\nabla c|$ conditional on c.

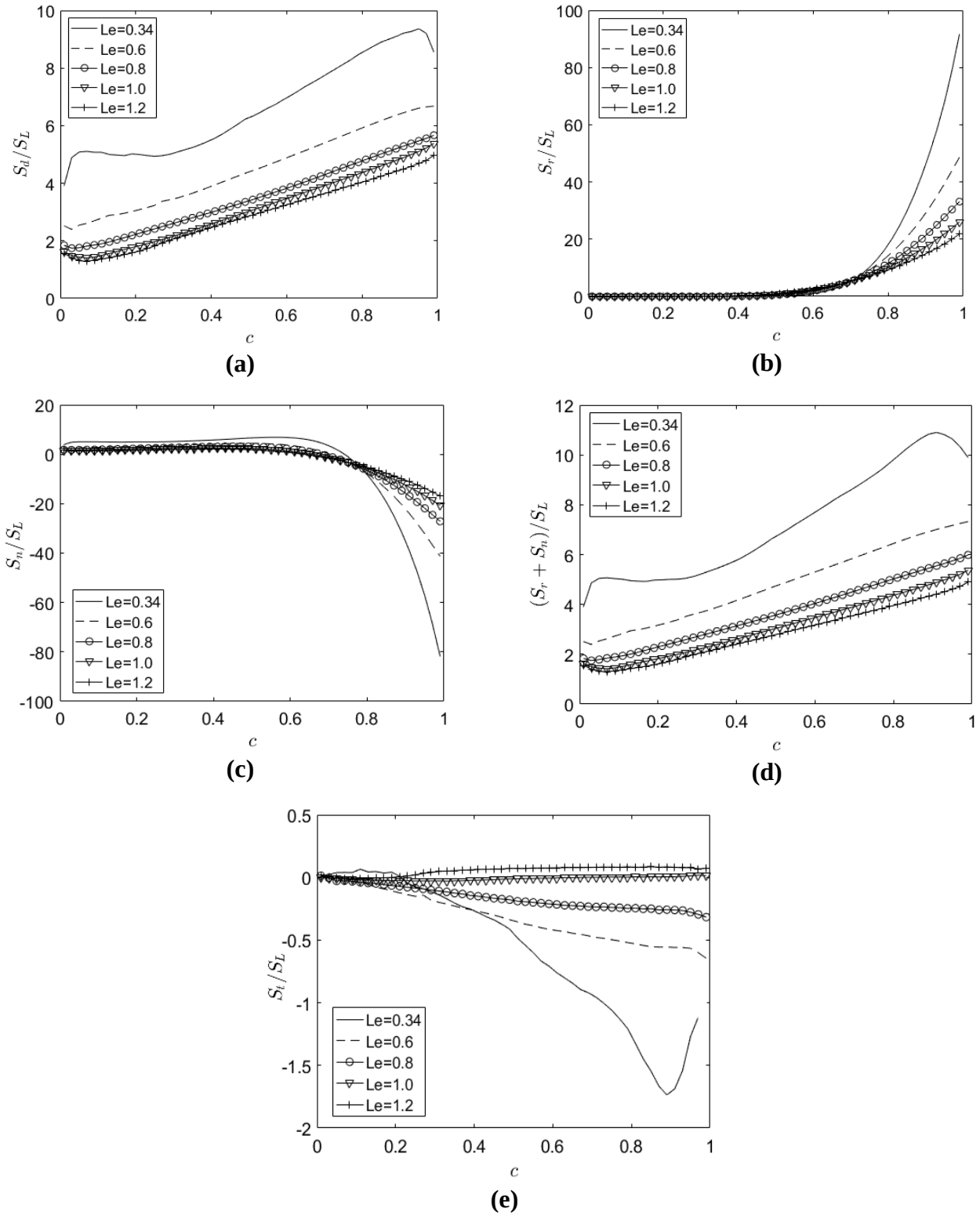

Figure 4: Variations of the mean values of (a) S_d/S_L, (b) S_r/S_L, (c) S_n/S_L, (d) $(S_r+S_n)/S_L$ and (e) S_t/S_L conditional on c for all cases considered here.

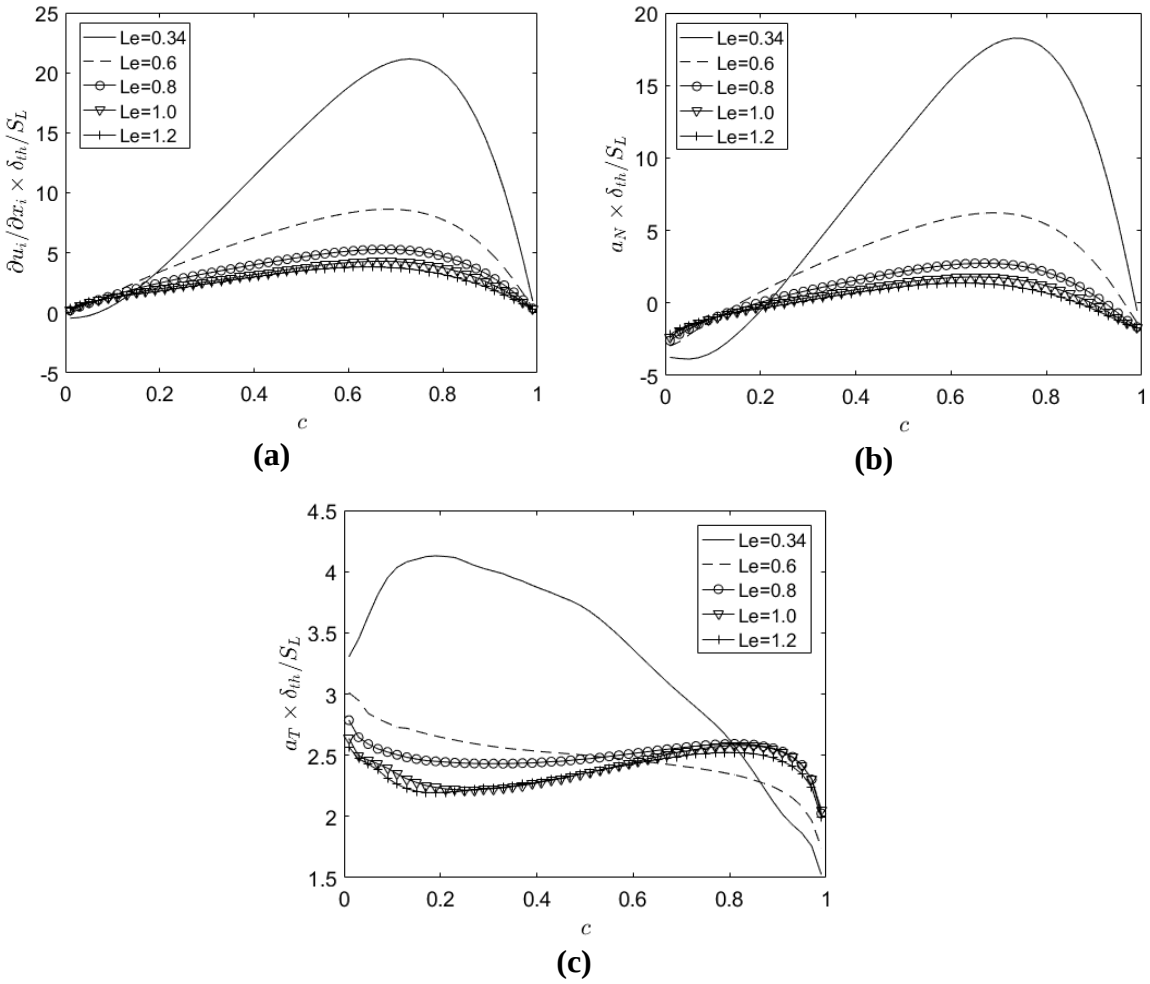

Figure 5: Variations of the mean values of (a) $\partial u_i/\partial x_i \times \delta_{th}/S_L$, (b) $a_N \times \delta_{th}/S_L$ and (c) $a_T \times \delta_{th}/S_L$conditional on c for all cases considered here.

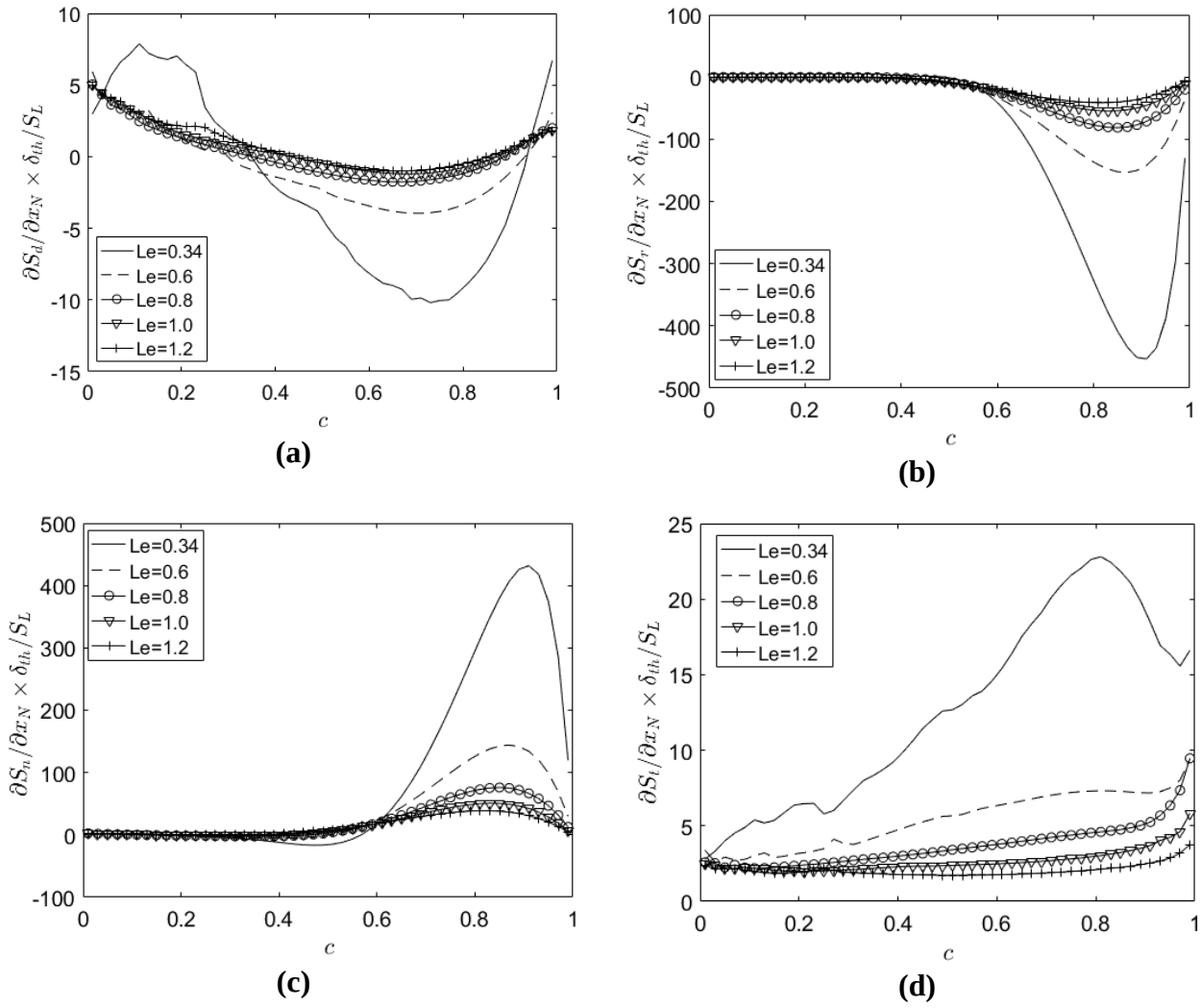

Figure 6: Variations of the mean values of (a) $\partial S_d/\partial x_N \times \delta_{th}/S_L$, (b) $\partial S_r/\partial x_N \times \delta_{th}/S_L$, (c) $\partial S_n/\partial x_N \times \delta_{th}/S_L$ and (d) $\partial S_t/\partial x_N \times \delta_{th}/S_L$conditional on c for all cases considered here.

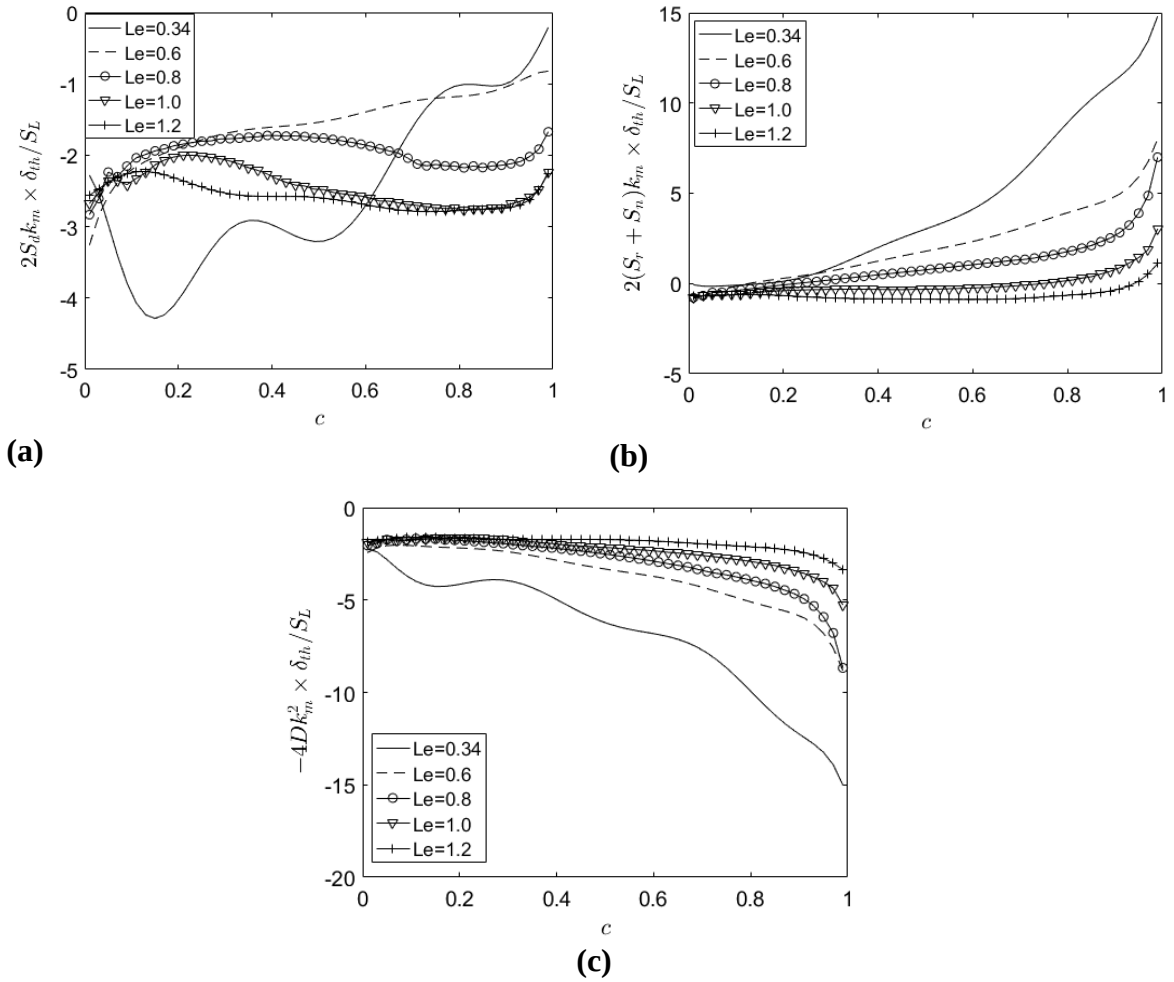

Figure 7: Variations of the mean values of (a) $2S_d k_m \times \delta_{th}/S_L$, (b) $2(S_r + S_n)k_m \times \delta_{th}/S_L$ and (c) $(-4Dk_m^2) \times \delta_{th}/S_L$conditional on c for all cases considered here.

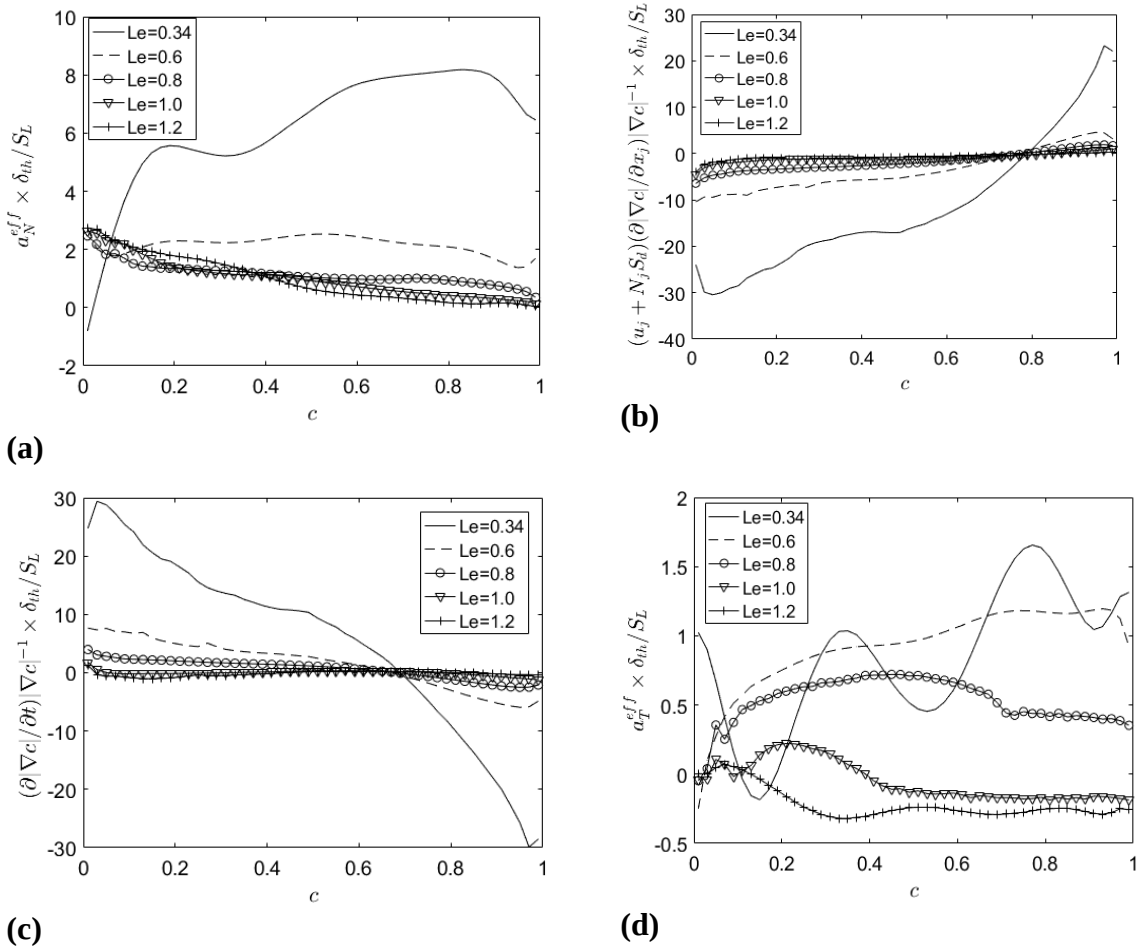

Figure 8: Variations of the mean values of (a) $a_N^{eff} \times \delta_{th}/S_L$, (b) $\{(u_j + S_d N_j)\partial|\nabla c|/\partial x_j\}|\nabla c|^{-1} \times \delta_{th}/S_L$, (c) $\{\partial|\nabla c|/\partial t\}|\nabla c|^{-1} \times \delta_{th}/S_L$ and (d) $a_T^{eff} \times \delta_{th}/S_L$conditional on c for all cases considered here.